Tectonophysics, 145 (1988) 141–156
Elsevier Science Publishers B.V., Amsterdam – Printed in The Netherlands

Evolution of fault patterns in clay experiments

Z. RECHES

Department of Geology, Hebrew University, Jerusalem 91904 (Israel)

(Received January 22, 1987; revised version accepted March 31, 1987)

Abstract

Reches, Z., 1988. Evolution of fault patterns in clay experiments. *Tectonophysics*, 145: 141–156.

The evolution of systems of strike-slip faults, from a single fault to intricate patterns, is examined here in a series of clay experiments. In the experiments, plates of clay are loaded laterally under constant strain rate in plane strain, with continuous monitoring of the stresses.

The experiments indicate that an individual fault appears as a linear trace, about 1 mm in length, that grows by in-plane propagation of one or both ends. Next, the fault evolves by out-of-plane propagation and interacts and coalesces with other, subparallel, faults. This process generates a crooked, nonlinear fault, which at this point usually ceases to grow. Younger faults developing close to the older fault may cross and displace it. The fault pattern in a sample changes in nature during a single run. The early pattern is either domainal or conjugate, depending on the initial fault distribution. The second stage is usually domainal when subparallel faults develop close to each other. During the final stage, young faults cross old ones and generate conjugate patterns.

The relation between rheology and growth mechanisms of the faults is discussed. Faults in brittle-elastic solids grow by out-of-plane propagation into zones of reduced normal stress, whereas many of the faults in the present experiments grow by in-plane propagation. This propagation direction and the fault pattern evolution, is interpreted here as indicating relaxation of nonuniform stresses at the proximity of the faults. It is further argued that stress relaxation may be applicable to faulting of rocks in the upper crust.

Introduction

Field observations indicate that faults occur in systems, forming patterns of several sets in two and three dimensions. The evolution of these patterns can be evaluated in the field from geometric relations observed in the *final* stage (Aydin and Johnson, 1978; Segall and Pollard, 1983). The present study provides experimental evidence for the *continuous* growth of faults and the *evolution* of complicated fault patterns.

The development of fault patterns is studied here in experimentally deformed clay samples. Clay samples are used for several reasons. First, it has long been known that fault patterns in clay models are similar to patterns in the field (Cloos, 1928; Tchalenko, 1970) and, further, previous clay experiments provided insight into the mechanics of faulting and fault-related deformation (Oertel, 1965; Hoppener et al., 1969; Hildebrand-Mittelfeldt, 1979). Second, it is difficult to observe the continuous, stable growth of faults in an intact rock sample, because unconfined rock samples, which can be photographically monitored, tend to yield unstably (Paterson, 1978). Third, the strain fields associated with faulting in clay are similar to those predicted by dislocation calculations, as demonstrated by Hildebrand-Mittelfeldt (1979). This similarity exists in spite of the apparent rheological difference between clay and the elastic continuum of the dislocation model.

The experiments show that initially isolated faults develop into complicated patterns, comprized of several sets, and consisting of fault zones,

0040-1951/88/$03.50

domains and conjugate sets. These patterns are interpreted as reflecting local stress relaxation due to the viscoelastic behavior of the clay. The applicability of this relaxation to naturally deformed rocks is discussed.

Observations in clay experiments

The experiments were run in a specially designed apparatus (Fig. 1) which produces uniform macroscopic strain within the samples due to its shear-free walls (Fig. 2). The apparatus is described in detail in Appendix 1. Forty tests were run with wet clay samples: 18 of these tests included continuous monitoring of the stresses (Appendix 1).

The geometric evolution of fault patterns is documented here; there is no intention to derive the quantitative parameters of faulting in clay. The large number of experiments was used primarily to examine cases under variable sample thickness and strain-rate conditions. It was found that growth mechanisms and pattern evolution were similar in all clay experiments, even though the patterns differ in detail from one experiment to the other. Eventually, a few experiments which clearly portray the pattern evolution were selected for presentation. In none of the tests do the observations contradict the general results summarized below. I first describe the development of individual faults and then the pattern evolution.

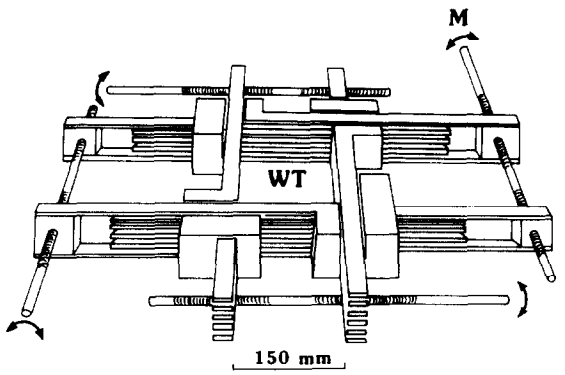

Fig. 1. The deformation frame of the experimental apparatus. Each side wall is composed of 11 slabs which slip with respect to each other.

Growth of a single fault

New faults form continuously during the experiments up to 20% of horizontal shortening. Newly formed faults are short and straight. The initial length of new faults is unknown, as faults shorter than 1 mm are not seen at the present resolution. It is likely, however, that the initial length is less than 1 mm, but no less than a few microns, the length of a clay particle. The number of faults and their cumulative length increase with deformation is discussed in detail in Reches (1986).

The new faults in the experiments trend between 12° to 35° on both sides of the axis of maximum compression (Fig. 3). The mean trend fluctuates from one stage to another with no clear tendency.

Some of the new faults did not change their length appreciably during the experiment, whereas others grew significantly longer. The growing faults are the active, dominant faults in the experiments and account for a large amount of the deformation. Two growth mechanisms have been recognized: *propagation* and *coalescence* (Fig. 4). Propagation is the extension of the fault from its ends into the unfaulted regions that surround it. In-plane propagation occurs in the same trend of the original fault (Fig. 4A), whereas out-of-plane propagation deviates from the original plane (Fig. 4B). Coalescence occurs when a small branch connects two subparallel faults, the ends of which are close to each other (Fig. 4C, D). The two faults join to become a longer fault composed of several segments in *en echelon* arrangement.

Figure 5 illustrates the geometry of several selected faults as they develop through four or five stages of each experiment. In all figures below, the axis of maximum compression was set to be in the N–S direction. Newly formed, short, straight faults grow primarily by *in-plane propagation*, as seen in faults 1 and 2 in Fig. 5a, faults 3 and 4 in Fig. 5b, faults 5 and 6 in Fig. 5c and fault 7 in Fig. 5d. These faults may grow as long as 20 mm by in-plane propagation, and presumably did so before they became visible. Furthermore, a fault may locally propagate out of its plane and later change its propagation direction to the original trend, as did fault 3 in Fig. 5b.

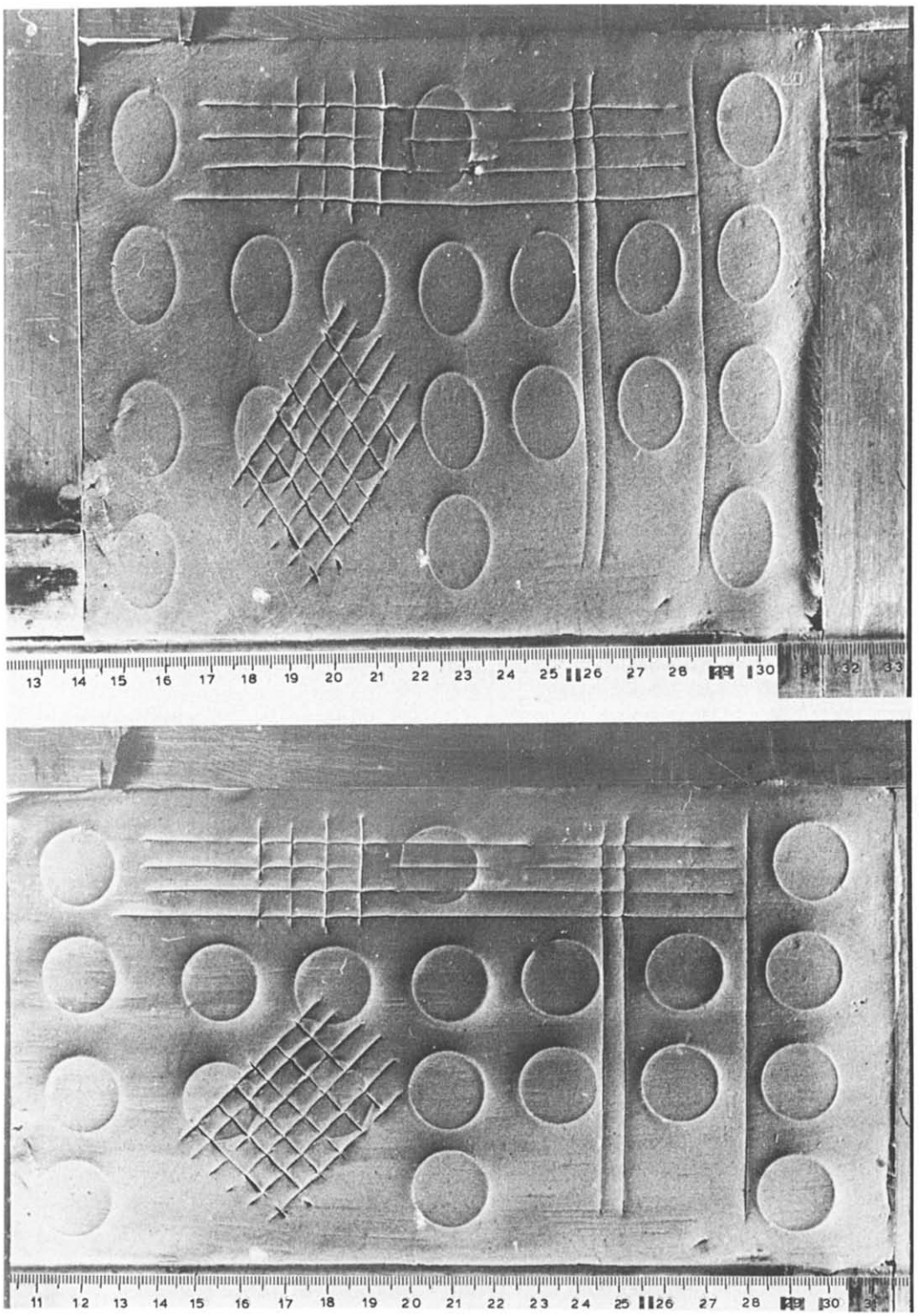

Fig. 2. Top view of a window putty sample deformed in the present apparatus. Scale marks in mm. A. Original sample. B. Sample after 21% shortening. Note the homogeneous deformation and the lack of shear along the side walls.

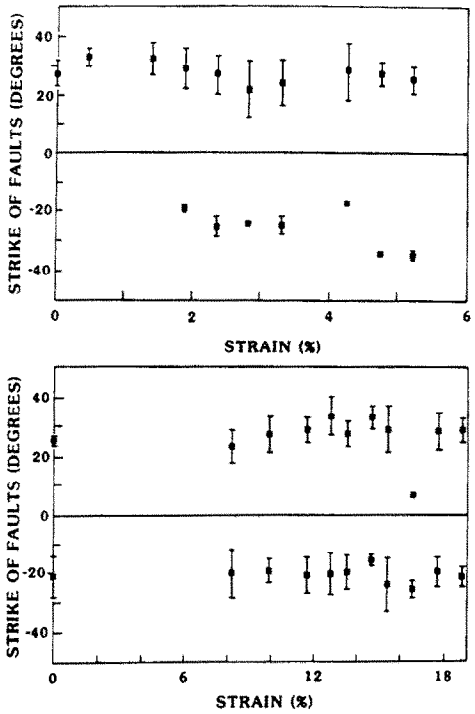

Fig. 3. Orientations of *new* strike-slip faults observed during different stages of two experiments. Orientations are shown as angles from the axis of maximum compression. Vertical bars, two standard deviations; short bar, or none, indicates measurement of only one or two new faults of the given stage.

When straight faults become 5–20 mm long, they tend to *propagate out-of-plane*, as did faults 2 and 8 in Fig. 5a, faults 6 and 9 in Fig. 5c and faults 7 and 10 in Fig. 5d. In some cases, the out-of-plane propagation causes a transition from strike-slip to oblique-slip.

The *coalescence* of faults occurs during all stages of fault development and involves various fault geometries and lengths (e.g, stage D in Fig. 5a, stage E in Fig. 5c and several cases in Fig. 5d). In the present experiments coalescence occurs pri-

Fig. 5. Examples of the growth of individual faults and some patterns. All figures are drawn after photographs of experiments. Horizontal dashed lines connect identical points of two separate stages. All experiments with a strain rate of 4×10^{-5} s^{-1}. Each figure displays several consecutive stages of an experiment with the following times (s) and finite strain (relatively to first stage A, in each ase.

a. (A) 0, 0; (B) 104, 0.004; (C) 207, 0.0083; (D) 300, 0.012.

b. (A) 0, 0; (B) 1150, 0.046; (C) 1575, 0.063; (D) 2425, 0.097.

c. (A) 0, 0; (B) 350, 0.014; (C) 575, 0.023; (D) 825, 0.033; (E) 1175, 0.047.

d. (A) 0, 0; (B) 125, 0.005; (C) 475, 0.019; (D) 700, 0.028.

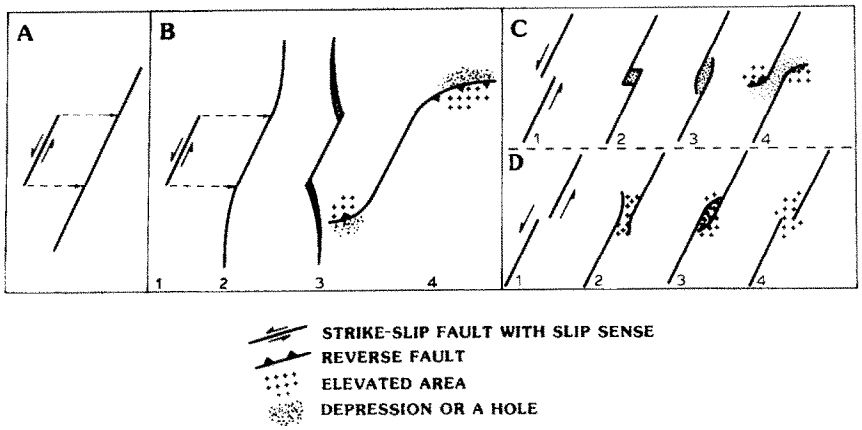

Fig. 4. Idealized modes of growth of strike-slip faults (after present experiments). A. In-plane propagation. B. Out-of-plane propagation: *1*—initial shape; *2*—gradual curving; *3*—extension crack growth; *4*—curving developing reverse faulting. C. Coalescence by dilational jogs (see text): *1*—initial shape; *2*—extension branches forming an idealized pull-apart basin; *3*—inward-curving oblique-normal faults; *4*—outward-curving oblique-reverse faults. D. Coalescence by antidilational jogs (see text): *1*—initial shape; *2*—outward-curving oblique faults; *3*—inward-curving oblique-reverse faults; *4*—a broad push-up region.

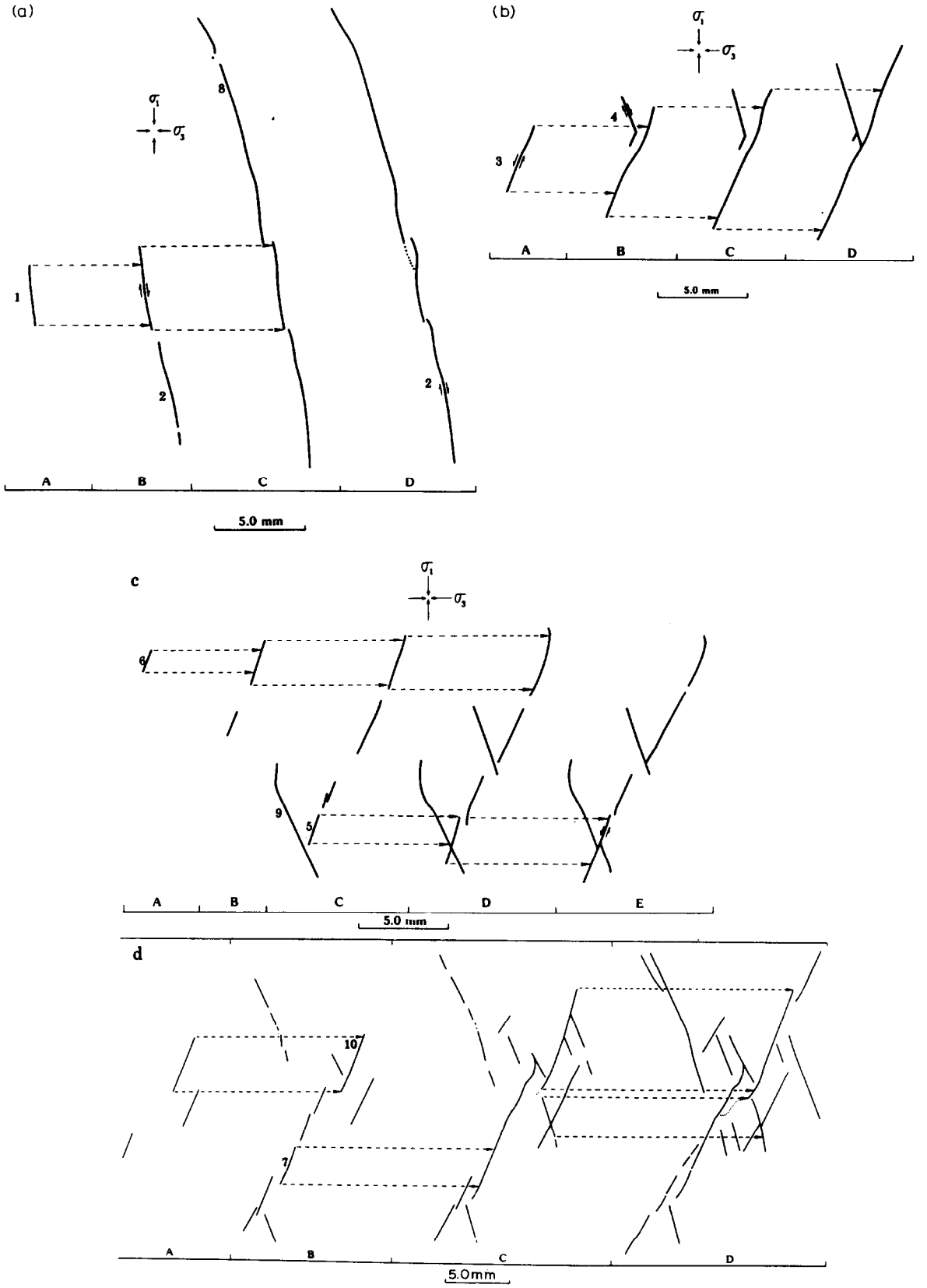
(a)
σ_1
σ_3
8
1
2
2
A
B
C
D
5.0 mm
(b)
σ_1
σ_3
4
3
A
B
C
D
5.0 mm
c
σ_1
σ_3
6
9
5
A
B
C
D
E
5.0 mm
d
10
7
A
B
C
D
5.0mm

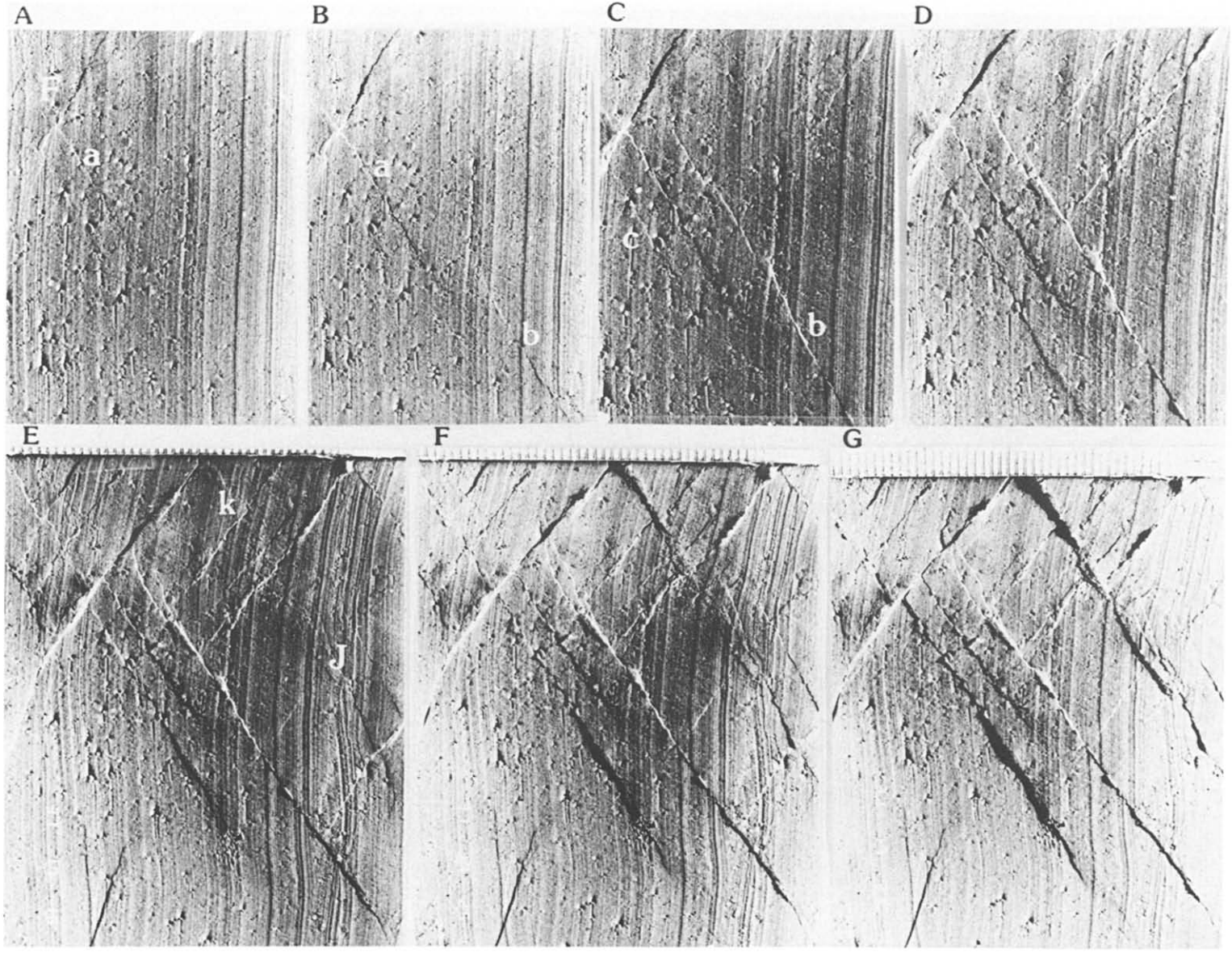

Fig. 6. Top view of the wet clay experiment D204 in seven stages. Maximum shortening N–S; the closely spaced N–S-trending striations are caused by the smoothing trowel; scale marks in (E)–(G) in mm. Strain rate 4×10^{-5} s^{-1}. Time (s) and finite strain values are as follows: (A) 1500, 0.06; (B) 1680, 0.0672; (C) 1800, 0.072; (D) 2040, 0.0816; (E) 2520, 0.101; (F) 2940, 0.1175; (G) 3420, 0.137. See text and Fig. 7.

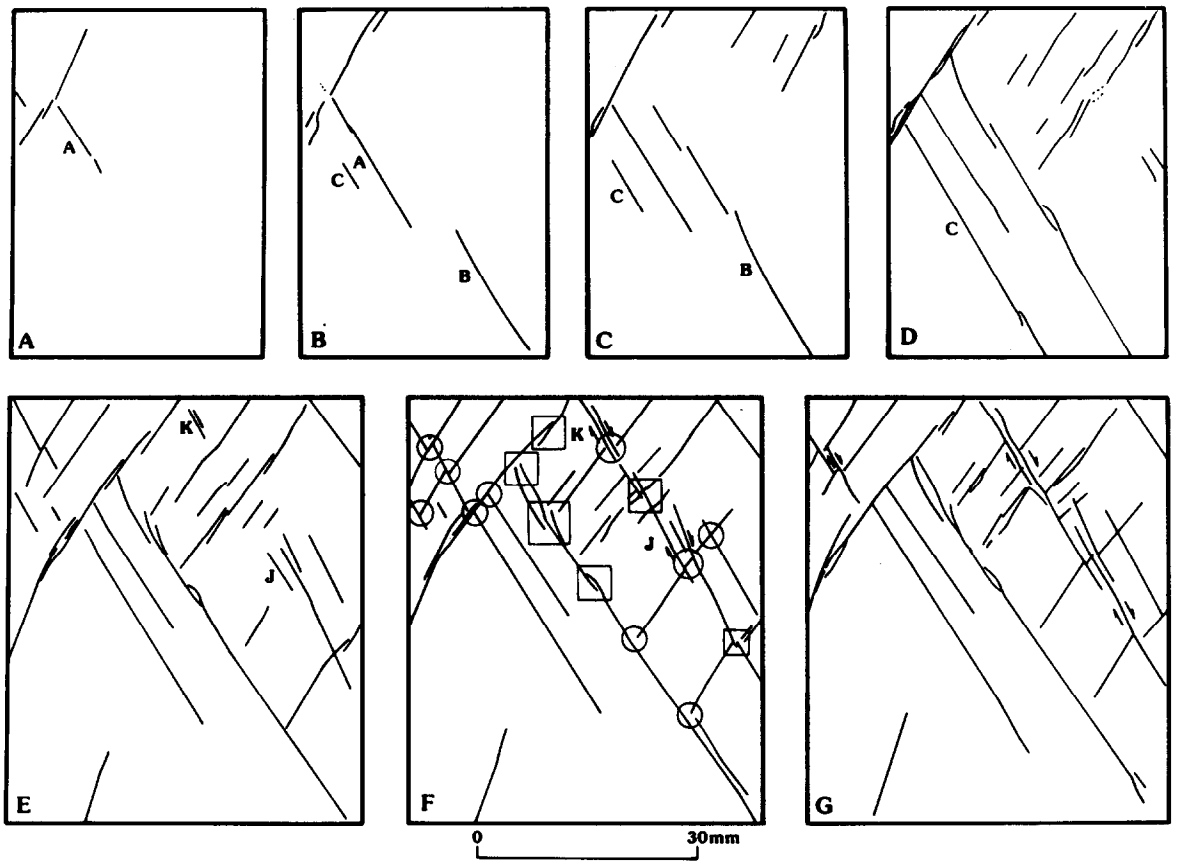

Fig. 7. Line drawings of the fault patterns shown in Fig. 6. Zones of proximity between faults are qualitatively classified in frame (F) into zones of interaction (squares) and zones of no interaction (circles) (see text).

marily by antidilational jogs. [Sibson (1985a) defines a dilational jog as a step that generates a hole, a pull-apart or a rhomb-shaped graben between the faults (Fig. 4C), and an antidilational jog as a step that generates a push-up or a horst (Fig. 4D).] The two coalescing faults bend *toward* each other and enclose the uplifted region, with steep oblique-reverse faults on all sides (jogs along the fault in Fig. 5a, stage D). The occurrence of antidilational jogs reflects primarily the initial en echelon distribution of the fault segments (e.g., Fig. 5a and fault 7 in Fig. 5d).

These growth processes lead to the development of a *mature* fault composed of several nonparallel or nonaligned segments and showing a crooked trace on map view (Fig. 5). The mature fault may be less active than newer faults (see the description of experiment D203 below).

The *interaction* between faults is recognized here by the deviation of a fault trace from its linear shape at the proximity of other faults. The interaction results are displayed for experiments D203 and D204, described in the following section (Figs. 6–9). Zones of proximity between faults in these experiments (Figs. 7 and 9) have been sorted into zones with and without interaction. Approximately the same number of zones occurs in both types in this qualitative estimate, with 13 interaction zones versus 16 noninteraction zones in stage F of Fig. 7 and stage C of Fig. 9. It appears that interaction is more common in zones of subparallel, overlapping segments in a fault zone (about 10 cases in the above figures) and less common in zones of fault intersections (only three cases). On the other hand, the majority of the noninteraction zones occur at fault intersections (Figs. 7 and 9).

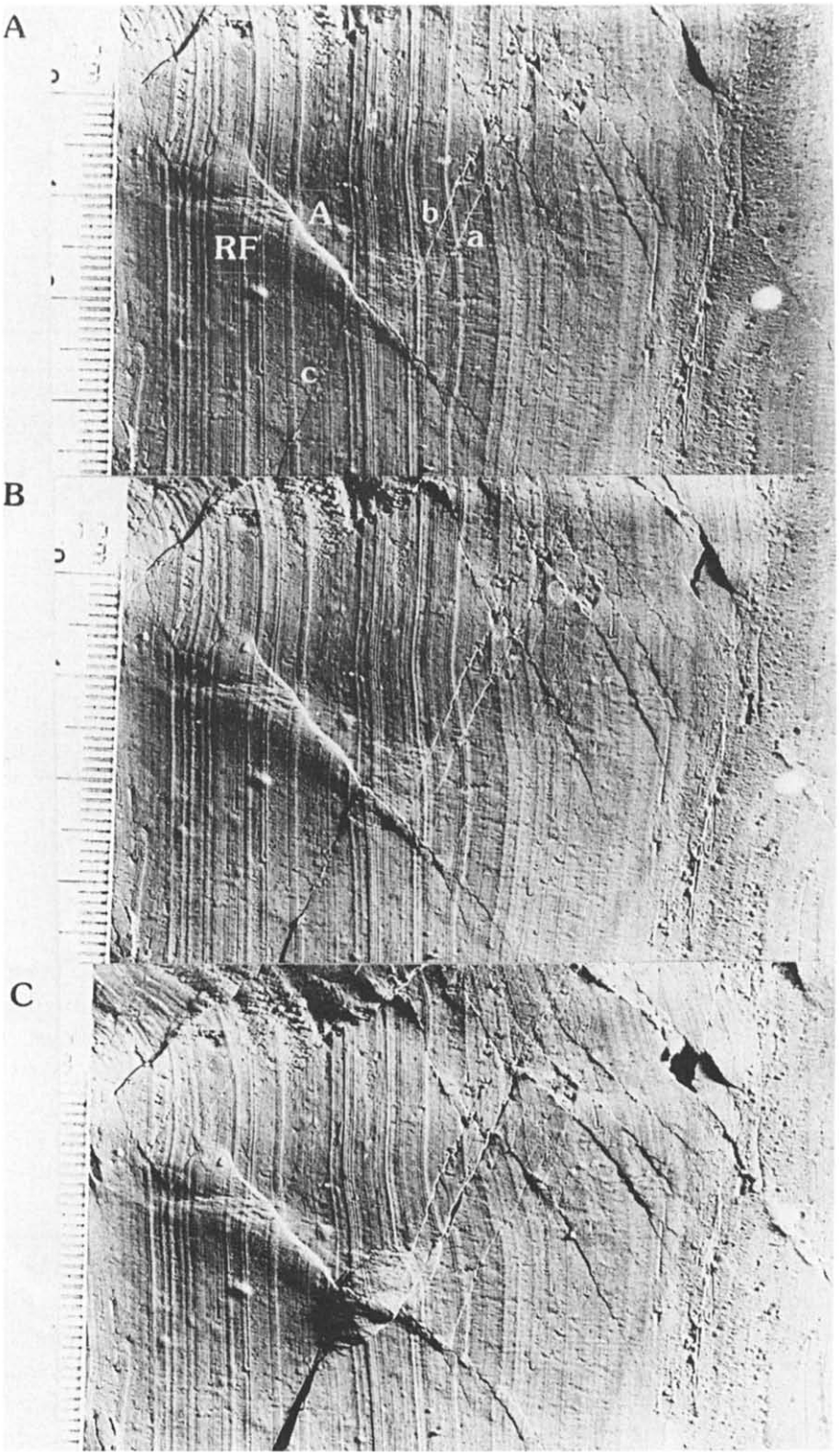

Fig. 8. Top surface of the wet clay experiment D203, in three stages. Maximum shortening N–S; the closely spaced N–S-trending striations are caused by the smoothing trowel; scale marks in mm. Strain rate 4×10^{-5} s^{-1}. Time (s) and finite strain values are as follows: (A) 1920, 0.0768; (B) 2220, 0.0888; (C) 3240, 0.129. See text and Fig. 9.

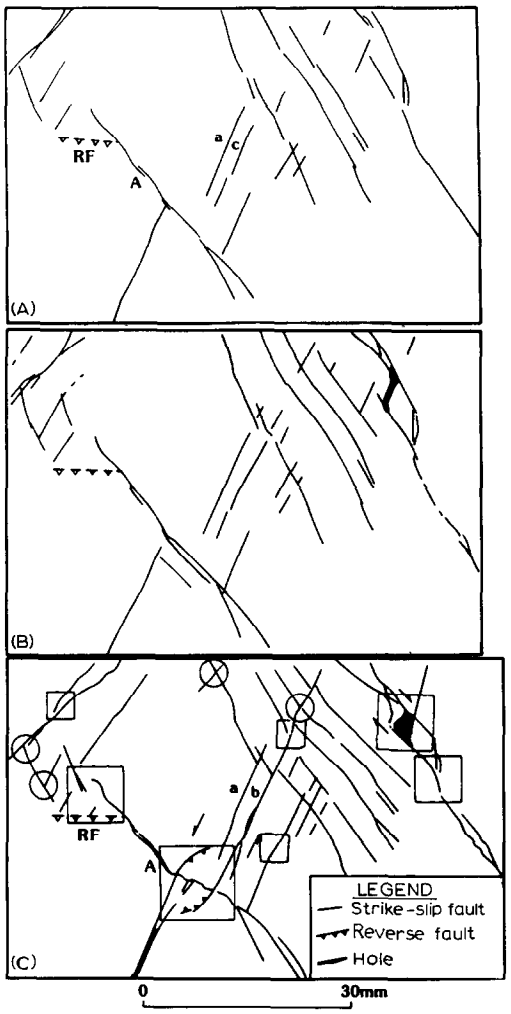

Fig. 9. Line drawings of the fault patterns shown in Fig. 8. Zones of proximity between faults are qualitatively classified in frame (C) into zones of interaction (squares) and zones of no interaction (circles) (see text).

Growth of a fault pattern

The growth of a pattern is described in detail for two selected experiments, and some general characteristics of the evolution are outlined.

In experiment D204 the initial clay sample was 57 mm high, 110 mm wide and 143 mm long. It was deformed at the rate of 4×10^{-5} s^{-1} at constant area. The first faults were detected visually after 4.5% shortening. The faulting in this experiment is shown in Fig. 6 (photographs), and Fig. 7 (fault map). In Fig. 6A a small linear fault marked *a*, trending N30° W, originated close to a much larger earlier fault, *F*, which trends N30° E. In Fig. 6B fault *a* has almost doubled its length and still remains linear. To the southeast of fault *a*, the new, subparallel fault *b* appears. Fault *b* continues as a linear feature until shortly before photo Fig. 6B was taken, then becomes slightly curved during propagation: its southeastern end trends N30° W, and its northwestern end trends N27° W. Figure 6C shows that fault *a* stops propagating; fault *b* propagates for a short distance, and two additional segments, in an echelon pattern, appear to the northwest of it. Figure 6D shows the three segments of fault *b* just before they combine and become one large fault, with several splays and small horsts at the steps. Fault *b* terminates against fault *F* by splaying and out-of-plane propagation (Fig. 6C, D). A third fault in this set, *C*, which is hardly visible in Fig. 6B and C, propagates almost linearly except for slight curving at its end (Fig. 6D).

The faults seen in Fig. 6A–D propagate initially and stop later. New faults form and propagate subparallel and close to still slipping and propagating older ones. In other words, the pattern develops *sequentially* rather than simultaneously. The sequence of development is shown in the series of the photographs (Fig. 6A–D), but it is impossible to determine the order of fault appearance from the final configuration alone (Fig. 6D).

During experiment D204 the type of fault pattern changes. In Fig. 6A and B several faults form a conjugate pattern which develops, in Fig. 6C and D, into two domains. Each domain includes three or four subparallel faults, NW-trending faults in the southwest corner and NE-trending faults in the northeast corner. The domainal pattern is also temporary. The small faults in groups *K* and *J* of Fig. 6E propagate and coalesce to form a large fault system, marked *K–J*, which cuts and displaces all pre-existing faults (Fig. 6G). The *K–J* system again generates a *conjugate* pattern in Fig. 6G. The final pattern (Fig. 6G) is a cumulative pattern which includes active faults, such as *K–J*, and some inactive ones, such as *a*. The inactive faults and the associated conjugate pattern may be

preserved, without obliteration, in the deforming clay to the end of the experiment, at about 20% of shortening in the horizontal direction.

The faulting in experiment D203 is shown in Fig. 8 (photographs) and Fig. 9 (fault maps). Maximum shortening is in the N–S direction and equal area is maintained. Figure 8A shows a portion of the sample after 7.7% shortening. The largest fault in the sample at this stage is the NW–SE-trending fault marked *A*, just left of center. This is a right-lateral fault which splays at its southeastern end, whereas its northwestern end is bent into a deeply buried reverse fault marked *RF*. The displacement along this fault is about 0.7 mm. In Fig. 8B, representing 8.9% shortening, the three faint linear faults *a*, *b* and *c* of Fig. 8A propagate and coalesce, forming a new NE–SW-trending zone which cuts and displaces the pre-existing fault *A*. Fault *A* still slips at its southeastern end, but does not at its center. The pattern changes from *domainal* in Fig. 8A to *conjugate* in Fig. 8C.

Experiment D203 also shows clear push-up and pull-apart structures between segments of a shear zone. The largest push-up structure appears in the center, in the overlapping region between faults *a*, *b* and *c*, which is also the intersection region with fault *A* (Fig. 8C). Note the topographic elevation and the reverse faults that encircle the push-up area. A few narrow holes along fault *a* (Fig. 8C) are pull-apart basins due to left steps along a left-lateral fault. The largest pull-apart structure appears first in the northeast corner of Fig. 8B, and it grows significantly between Fig. 8B and C. The origin of this basin can be noticed already in the depressed topography in Fig. 8A (discussed in Reches, 1987).

Are there any early indications in Fig. 8A that fault *A* is going to become inactive, whereas faults *a*, *b* and *c* are going to form the most active zone? One possible clue is in the geometry of fault *A*. In Fig. 8A it is already splayed and bent at both its ends. This is probably an advanced stage in the life cycle of a fault and, although further slip may occur along bent or splayed faults, this is not likely. On the other hand, the three faults *a*, *b* and *c* are straight in Fig. 8A and, thus, are probably in an earlier stage of their development.

Summary: evolution of a fault pattern

The multi-fault patterns display an evolution in approximately the following sequence. First, small faults form at one or two locations within the central part of the clay sample. The initial faults trend between 12° to 35° from the direction of maximum compression, and they display a conjugate or a small domain of subparallel faults (stage (A) in Fig. 7). Second, the small faults grow longer and form a conjugate pattern or a domainal pattern, most likely depending on the original pattern. The original faults remain the most visible, though not the most active or the fastest growing. In many experiments the initial faults stop propagating and slipping and remain inactive to the end of the test (Fig. 7).

New faults continue to appear during the experiment and, in the third stage, some of the new faults cut old faults and change the nature of the pattern (Figs. 6–9). Finally, in a late stage of some experiments, one fault may become dominant and turn into an active shear zone which accommodates most of the slip (Figs. 6E–G, 8B, C). The fault patterns are cumulative and reflect the increase in the number of the faults and their growth.

The stresses during the experiments

The normal stresses within the deforming clay samples were monitored continuously during 18 out of 40 tests, by a system of pressure gauges that measure the average horizontal stresses in the clay (Appendix 1). This section presents the experimental maximum shear stress, $\tau_{max} = (\sigma_x - \sigma_y)/2$, where σ_x and σ_y are the normal horizontal stresses measured parallel to the axes of maximum and minimum compression of the apparatus, respectively.

Figure 10 displays the time variations of the shear stresses during several experiments with constant strain rate. Four stages can be distinguished in the stress–time curves, as follows.

Stage a is an initial stage, characterized by low shear stresses (Fig. 10A, B, C). When an experiment was stopped for technical reasons and was resumed after several minutes, this stage did not recur and the shear stresses rose rapidly (Fig.

10D). Stage *a* is probably due to a mismatch between the gauges and the clay, or some other artefact of the experiments.

Stage b occurs in a similar fashion in almost all experiments. The shear stress rises initially at a high rate, followed by a lower rate (Fig. 10). The stress rise during this stage may be monotonous (Fig. 10B) or in steps (Fig. 10A and C).

Stage c. In most experiments, the rising shear stresses approach a nearly stable level of about 1000–2700 Pa (Fig. 10A, B, C, D). Detailed examination of the stresses during this stage reveals temporary phases of hardening and softening (Fig. 10E). In the hardening and softening phases, the shear stress rises or drops as much as 200 Pa from the mean. These temporary stress variations are observed in plots of running averages, which eliminate inconsistent noise.

Stage d. Stopping the motors causes the onset of stress relaxation (Fig. 10A, C, F) with an exponential decay curve; the shear stresses relax to a finite level and do not vanish entirely.

The shear stress variations shown by Oertel (1965) are similar to those described here (Fig. 10F), although he used a different apparatus and a different clay. This similarity suggests a deformation mechanism common to all clays, as discussed below.

Discussion

Fault growth and rheology

Faults in the present samples grew by several mechanisms: in-plane propagation (Fig. 4A); out-of-plane propagation (Fig. 4B); and coalescence with subparallel faults (Fig. 4C, D). The relationship between these growth mechanisms and the rheology of the host medium is first discussed.

Fault growth in an elastic solid

The stresses at the proximity of a fault em-

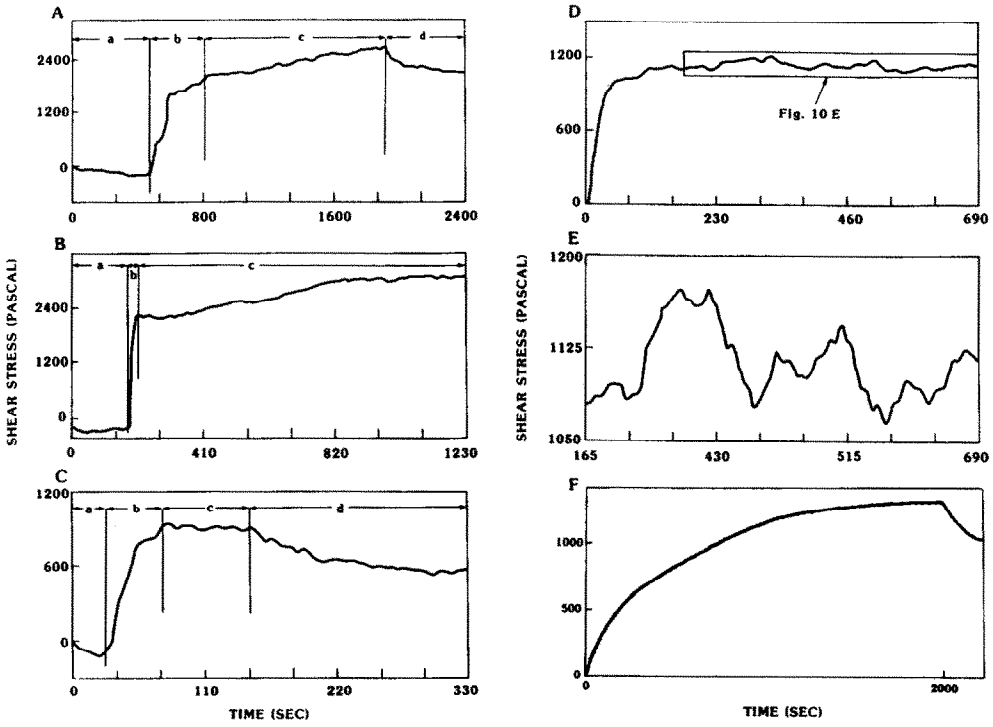

Fig. 10. Variations of τ_{max} with time in several experiments. The stages *a* to *d* are discussed in the text. Note different scales of time and stress; strain rate $= 4 \times 10^{-5}$ s^{-1}. (A) Experiment D220; (B) experiment D200; (C) experiment D221, first phase; (D) experiment D204; (E) detail from (D), showing short-term stress variations; (F) shear stresses of the compression experiments by Oertel (1965, after Fig. 13).

bedded in an elastic solid may be separated into two components; a uniform stress generated by a remote source, and a local, nonuniform stress generated by the slip along the fault. The nonuniform stress which perturbs the uniform stress field includes zones of increased or reduced shear stress, and zones of increase or reduced normal stresses (Anderson, 1951; Chinnery, 1966; Lawn and Wilshaw, 1975; Segall and Pollard, 1980). The dimensions of these zones and the magnitude of the stress increase (or decrease), depend on the magnitude of the slip and its distribution along the fault (e.g., Chinnery, 1966).

The nonuniform stresses are particularly intense at the fault termination zones and, thus, these stresses modify the direction of the fault propagation. The direction of propagation was studied in experiments with samples of unconfined plates of rocks and other elastic material, cut by a single or several elongated fractures (Fig. 11) (Brace and Bombolakis, 1963; Lawn and Wilshaw, 1975; Ingraffea, 1981; Horii and Nemat-Nasser, 1985). These fractures are oblique to the principal stresses and thus are subjected to shear stresses parallel to their long axes. In *all* the experiments of this type the fractures propagate from the termination zones as extension cracks into the regions of *reduced mean stress*, $(\sigma_1 + \sigma_3)/2$ (Fig. 11 and Fig. 4B, case 3) (Lawn and Wilshaw, 1975; Ingraffea, 1981; Horii and Nemat-Nasser, 1985).

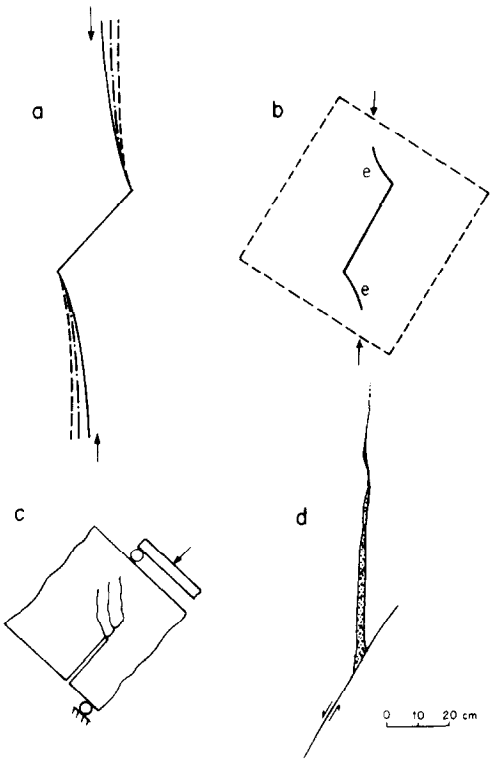

Fig. 11. Off-plane fault propagation in brittle-elastic solids. Maximum compression is vertical; initial faults trend in an NE–SW direction. a. Fault in a Columbia resin CR39; solid, subvertical lines are observed propagated cracks, and dashed lines are calculated propagation paths (after Horii and Nemat-Nasser, 1985). b. Extension of a fault in glass as extension cracks, marked *e* (after Brace and Bombolakis, 1963). c. Fracture paths in a sample of Westerly granite under mixed normal and shear stresses (after Ingraffea, 1981). d. Extension crack in granite in the Sierra Nevada (Segall and Pollard, 1983).

Fault growth in a viscoelastic material

Consider a fault slipping at a constant slip-rate, which is embedded in a Maxwell material. The nonuniform strain-rate associated with the fault slip generates nonuniform stresses at the fault tip, similar in distribution to the stresses in an elastic solid. The shear stresses in a Maxwell material relax exponentially with time; the rate of this relaxation is characterized by the *relaxation time*, defined as the ratio of the viscosity to the shear modulus. Thus, one anticipates that nonuniform stresses could relax in a Maxwell material (McClintock and Argon, 1966, p. 547).

In a material with a short relaxation time relative to the fault slip-rate, the nonuniform stresses relax fast, and the fault grows in an almost uniform stress field (the same field which drives the deformation and causes faulting). Under such a uniform field, the fault should propagate in its initial plane without orientation changes. In a material with a long relaxation time relative to the fault slip-rate, the nonuniform stresses relax only partially, and the fault should propagate similarly to a fault propagating in an elastic solid (McClintock and Argon, 1966, p. 547).

Therefore, a fault in a viscoelastic material propagates in either a uniform stress field or a nonuniform stress field, depending on the relationship between the fault slip-rate and the relaxation time of the host material. Similar arguments were raised by Kanninen and Popelar (1985, section 7.4) for the energy calculation for the growth of an extension crack in a viscoelastic material

(their eqns 7.4-3, 7.4-4), and by McClintock and Argon (1966, ch. 17) in their discussion on transitional modes of fractures.

Fault growth in the present clay experiments

Some of the observations in the present experiments differ from the observations in elastic solids. First, most new faults have linear traces and many propagate colinearly with their initial trends (Figs. 5, 6, and 8). Further, in several cases, a linear fault trace that started to bend corrected itself onto its original trend (Fig. 5a). Second, many young faults propagate near large, active faults without changing their orientations, and young faults sometimes cut and displace old ones (Figs. 6–9). Third, the orientations of new faults is constant during the experiments (Fig. 3), and thus they are independent of the existence of older faults as well as the cumulative finite strain.

These observations indicate, on one hand, that the growing faults are related to the orientations of the principal stress axes generated by the deformation apparatus and, on the other hand, that the growing faults are not affected by nonuniform stresses generated by themselves or by other faults.

The most reasonable mechanism to maintain such uniform orientations of the stress axes during the experiments is local relaxation of the nonuniform stresses at the proximities of the faults.

Relaxation is evident in the present experiments: shear stresses in the clay samples decrease after the motors are stopped (stage *d* in Fig. 10); similar relaxation also occurs in the experiments of Oertel (1965) (Fig. 10f). The relaxation of the clay samples reflects the viscoelastic component of clay rheology, which has been analysed previously (e.g., Mitchell et al., 1968; Singh and Mitchell, 1968; Bazant et al., 1975; Bazant and Kim, 1986). These authors modeled the macroscopic rheology of clay by considering the microscopic mechanisms of slip, and breakage of the bonds between the clay particles. The rate of slip of the particles, and the corresponding macroscopic strain rate, are assumed to be controlled by the activation energy of the interparticle bonds (Bazant and Kim, 1986). These models yield constitutive laws with three parameters of linear and nonlinear viscoelastic modes (Mitchell et al., 1968).

While the complex rheology of clay is beyond the scope of this study, the viscoelastic mode in clay seems to explain the main observations of fault growth in the present experiments.

However, the present clay samples display *two mode* of fault geometry. On one hand, as discussed above, many fault traces show in-plane linear growth, indicating stress relaxation and no fault interactions (Figs. 5, 6 and 8). But on the other hand, other fault traces are curved, propagate out-of-plane or curve close to large neighbors, indicating no stress relaxation and fault interaction (Figs. 7F and 9C).

Such coappearance of the two modes may be attributed to inhomogeneities of the sample strength and loading system. However, such coappearance may also be assigned to relations of fault slip-rate and stress relaxation rate in an homogeneous clay. The relaxation rate can be estimated from the decay of the shear stresses during stage d of the experiments (Figs. 10A, B, C). The linearized relaxation rate ranges from about 3.5% in 100 s (Fig. 10A) to about 20% in 100 s (Fig. 10C). As the duration of the experiments is hundreds to thousands of seconds (Fig. 10), it is likely that the nonuniform stresses due to the slip along the faults are only partly relaxed. Thus, the fault traces in the clay experiments display mixed geometry, from the linear traces predicted for a uniform stress field to the curved traces predicted for a nonuniform stress field.

The mechanisms of fault growth in the present experiments are interpreted as indicators of complete or partial relaxation of nonuniform stresses at the fault proximities. This stress relaxation is attributed here to the viscoelastic mode of clay rheology, which has been derived previously in investigations based on interparticle bonds (see above). *Therefore, the present study leads to the hypothesis that the geometry of fault patterns, including orientations, positions, propagation directions and evolution in time, is a plausible indicator of material rheology.*

Possible application to faults in the field

The geometry of faults in the field has been previously analysed in terms of fractures in an

elastic solid (e.g., Anderson, 1951; Hafner, 1951), plastic slip surfaces (e.g., Ode', 1960), slip surfaces between rigid blocks (e.g., Freund, 1974; Garfunkel, 1974; Reches, 1978), or reactivated extension fractures in a brittle solid (Segall and Pollard, 1983). The present study suggests that the *viscous* mode of upper crustal rocks may account for some of the geometric features of faults and for the similarity of patterns between clay experiments and faulted rocks.

The application of this concept to planar faults in the field is not obvious: Could viscoelastic stress relaxation occur at large faults in the field? If such relaxation happens, the reduction of the nonuniform stresses may lead to in-plane fault propagation in rocks. Two indications of time-dependent stress relaxation in upper crustal rocks are presented here to demonstrate the feasibility of such processes.

Sibson (1985b) studied the occurrence of aftershocks around fault termination zones and in regions of jogs. He proposed that these aftershocks indicate brecciation associated with the stress field off the main fault. Now, suppose that fast slip occurs along an existing fault, and nonuniform stresses are generated at the fault termination. These stresses are insufficient for fault growth, but they are sufficient to brecciate the rocks close to the fault termination. Eventually, the nonuniform stresses partly relax, as indicated by the exponential decay of the number of aftershocks. Thus, brecciation is one possible process for macroscopic stress relaxation.

The viscoelastic parameters of large, intact beams of granite and gabbro were measured under low-temperature and low-pressure conditions (Ito, 1979; Ito and Sasajima, 1980). In a series of experiments, some lasting up to 20 years, these authors measured the strain-rate of rock beams subjected to shear stresses of a few tens of bars at room temperature and pressure. They found that the strength of granite diminishes until it behaves as a Maxwell material with viscosity of $1\text{–}6 \times 10^{20}$ Poise under a strain rate of 6×10^{-14} s^{-1} (Ito and Sasajima, 1980). Gabbro, on the other hand, did not flow.

Thus, viscoelastic flow may reduce nonuniform stresses in the crust where granite and other rocks are wet, fractured and at an elevated temperature, and have even lower viscosity than calculated by Ito and Sasajima (1980). According to the present hypothesis, it is likely that various viscosity mechanisms of crustal rocks and the associated stress relaxations control the fault geometry in the field.

Conclusions

The present study provides the detailed experimental results on the evolution of fault patterns which can be summarized as follows:

(1) Small, new, straight faults form during the entire experiment.

(2) Some faults maintain their original length and shape until the end of the experiment.

(3) Other faults grow first by in-plane propagation, then by out-of-plane propagation and coalescence. Eventually, long, crooked faults become inactive and are displaced by younger, active ones.

(4) The orientations and shapes of new faults are independent of the total strain and are, in general, not influenced by the pre-existing faults

(5) Interaction between faults is relatively common in regions where closely spaced subparallel faults overlap each other, and less common in regions where faults of different orientations intersect each other.

(6) Fault patterns are the result of the continuous accumulation and growth; no events of fast faulting have been observed.

(7) A master fault that is active may develop from a pre-existing fault and may dominate deformation in late stages of the experiments.

(8) The clay samples underwent stress relaxation, as is evident from the stress measurements after stopping the motors.

The proposed interpretation is that the geometry of the patterns is affected by the viscoelastic mode of the clay, which allows local stress concentrations around the faults to relax, and makes the in-plane propagation of the faults possible. This interpretation may be applicable to faulting of rocks in the field.

Acknowledgements

I benefited from discussions with David D. Pollard, Zvi Garfunkel, Paul Segall, Gerhard

Oertel, Don Ragan and Yonathan Erez. The deformation apparatus was built by Ittai Peles and Eliezer Gill of the Hebrew University, Jerusalem; their work is greatly appreciated. Thanks to Roni Ben-Ari and Avi Burg for their technical assistance. The reviews and comments of Paul Delaney, Paul Segall and Jon Fink contributed to the manuscript. The comments and suggestions of Gerhard Oertel, David D. Pollard, Mel Friedman and Ray C. Fletcher significantly improved the manuscript. Nevertheless, the above-mentioned people do not necessarily agree with the content of the study. The research was supported by a research grant from the Hebrew University, Jerusalem.

Appendix 1

Experimental set-up

The deformation apparatus is built for samples up to 57 mm high and up to 210 mm wide and long (*WT* in Fig. 1), with control and monitoring executed by an Apple II computer. Displacements are applied by the side walls, all four of which are built from 11 interchangeable slabs. During the deformation, each slab moves in a direction opposite to its upper and lower neighbors. In this arrangement, the gross shear traction along the walls is eliminated. Shear-free side walls produce uniform strain in the sample (Fig. 2).

The displacement of the side walls are applied by four motors (*M* in Fig. 1) capable of generating strain rates from 4×10^{-6} s^{-1} to 4×10^{-5} s^{-1}. The clay samples are deformed under conditions of continuous, coaxial pure shear in which the horizontal area of the samples is maintained constant. The strain-rate and the area are controlled by continuous adjustment of the velocity of the side walls. A sequence of black and white photographs is taken during each experiment. The clay used for most experiments was Motza Marl, a Cenomanian marl of the Judean Hills, Israel.

In a typical experiment, the clay is molded into the apparatus space, filling the complete 57 mm height of the apparatus, and is loaded only by the shear-free side walls. Alternatively, in some experiments, the clay is molded on top of a 20–30 mm thick substratum made of window putty. The window putty deforms uniformly up to about 35% of finite compression (Fig. 2). Under these conditions, the clay sample is confined by both the shear-free side walls and the uniformly deforming substratum. Clay samples were shortened up to 20% parallel to the maximum compressive axis without major detachments from the side walls.

Usually, the early faults appear near the side walls and close to the stress gauges. However, only the faults which develop at a distance from any apparent stress concentrator are examined in detail. These faults appear after 5–6% of shortening in the direction of the maximum compressive axis. Once an initial fault is observed, the camera is adjusted for a close-up view of the sample.

The stress measurements

The stresses accompanying the deformation are monitored by three pressure gauges made by Kyowa (Japan). These are small disks, 6 mm in diameter and 0.5 mm thick, with built-in membrane and strain gauges that measure the pressure normal to the membrane with ± 100 Pa accuracy. The spatial variation of the stresses in the clay samples was examined in a series of tests, not reported here, in which the three stress gauges were emplaced parallel to each other in several configurations of spacing, depth and position in the apparatus. The measured difference between the various positions appears small when the gauges are at least 20 mm away from the side walls and at least 10 mm deep. The measured stresses are not affected by proximity to small and intermediate-size faults. In a few cases, however, a *large* fault which cuts across the gauge site detaches the gauge from its enclosing clay; in such a case, the recorded stresses have been disregarded. For the undisturbed runs, the measured pressures are regarded as representative of the mean stress in the clay normal to the gauge surface.

During the experiments the stresses are monitored as follows. Two gauges are emplaced in the sample, close to each other and about 30–40 mm away from the side walls. One gauge is normal to x, the maximum compression axis, and the other is normal to y, the maximum extension axis of the

apparatus. A third gauge is emplaced in a separate clay specimen from the batch of the sample, but in an undeforming box. The third gauge serves as a control for stresses due to the drying of the wet clay and the noise of the monitoring system. Stresses are measured in 0.2 s intervals, and the mean value of 25 separate readings is recorded. All stresses are set to zero at the start of each experiment. The stresses measured by the third gauge are subtracted from the horizontal stresses, to obtain σ_x and σ_y. The shear stress, $\tau_{max} = (\sigma_x - \sigma_y)/2$, is calculated for the entire experiment.

References

Anderson, E.M., 1951. The Dynamics of Fault and Dike Formation with Applications to Britain. Oliver and Boyd, London, 206 pp.

Aydin, A. and Johnson, A.M., 1978. Development of faults as zones of deformation bands and as slip surfaces in sandstone. Pure Appl. Geophys., 116: 931–942.

Bazant, Z.P., Ozaydin, K. and Krizek, R.J., 1975. Micromechanisms model for creep of anisotropic clay. J. Engng Mech. Div., ASCE, 101: 57–78.

Bazant, Z.P. and Kim, J.-K., 1986. Creep of anisotropic clay: microplane model. J. Geotech. Eng., ASCE, 112: 458–475.

Brace, W.F. and Bombolakis, E.G., 1963. A note on brittle crack growth in compression. J. Geophys. Res., 68: 3709–3713.

Chinnery, M.A., 1966. Secondary faulting. 1. Theoretical aspects. Can. J. Earth Sci., 3: 162–174.

Cloos, H., 1928. Experimente zur inneren Tektonik. Zentralbl. Mineral. Geol. Palaeontol., pp. 609–621.

Freund, R., 1974. Kinematics of transform and transcurrent faults. Tectonophysics, 21: 93–134.

Garfunkel, Z., 1974. Model for the Late Cenozoic tectonic history of the Mojave desert, California, and for its relation to adjacent regions. Geol. Soc. Am. Bull., 85: 1921–1944.

Hafner, W., 1951. Stress distribution and faulting. Bull. Geol. Soc. Am., 62: 373–398.

Hildebrand-Mittelfeldt, N., 1979. Deformation near a fault termination, Part I. A fault in a clay experiment. Tectonophysics, 57: 131–150.

Hoppener, R., Kalthoff, E. and Schrader, P., 1969, Zur physikalischen Tektonik: Bruchbildung bei verschiedenen Deformationen in Experiment. Geol. Rundsch., 59: 179–193.

Horii, H. and Nemat-Nasser, S., 1985. Compression-induced microcrack growth in brittle solids: axial splitting and shear failure. J. Geophys. Res., 90: 3105–3125.

Ingraffea, A.R., 1981. Mixed-mode fracture initiation of Indiana limestone and Westerly granite. Proc. U.S. Symp. Rock. Mech., 22nd, pp. 186–191.

Ito, H., 1979. Rheology of the crust based on long-term creep tests of rocks. Tectonophysics, 52: 629–641.

Ito, H. and Sasajima, S., 1980. Long-term creep experiment of some rocks observed over three years. Tectonophysics, 62: 219–232.

Kanninen M.F. and Popelar, C.L., 1985. Advanced Fracture Mechanics. Oxford University Press, Oxford, 563 pp.

Lawn, B.R. and Wilshaw, T.R., 1975. Fracture of Brittle Solids. Cambridge University Press, Cambridge, 204 pp.

McClintock, F.A. and Argon, A.S., 1966. Mechanical Behavior of Materials. Addison-Wesley, Reading, Mass., 770 pp.

Mitchell, J.K., Campanella, R.G. and Singh, A., 1968. Soil creep as a rate process. J. Soil Mech. Engng Found., ASCE, 94: 231–253.

Ode', E., 1960. Faulting as a velocity discontinuity in plastic deformation. In: Rock Deformation. Geol. Soc. Am. Mem., 79: 293–321.

Oertel, G., 1965. The mechanics of faulting in clay experiments. Tectonophysics, 2: 343–393.

Paterson, M.S., 1978. Experimental Rock Deformation—The Brittle Field. Springer, New York, N.Y., 254 pp.

Reches, Z., 1978. Analysis of faulting in three dimensional strain field. Tectonophysics, 47: 109–129.

Reches, Z., 1986. The development of a fracture network by shear: experimental results. Symp. Rock Mech., 27th, Alabama.

Reches, Z., 1987. Mechanical aspects of pull-apart basins and push-up swells with applications to the Dead Sea transform. In: Z. Ben-Avraham (Editor), Sedimentary Basins within the Dead Sea and Other Rift Zones. Tectonophysics, 141: 75–88.

Segall, P. and Pollard, D.D., 1980. The mechanics of discontinuous faults. J. Geophys. Res., 85: 4337–4350.

Segall, P. and Pollard, D.D., 1983. Nucleation and growth of strike slip faults in granite. J. Geophys. Res., 88: 555–568.

Singh, A. and Mitchell, J.K., 1968. General stress–strain-time function for soils. J. Soil Mech. Eng. Found., ASCE, 94: 21–76.

Sibson, R.H., 1985a. Stopping of earthquake ruptures at dilational fault jogs. Nature, 316: 248–251.

Sibson, R.H., 1985b. Earthquake rupturing and brecciation processes in crustal fault zones, (abstract). Eos, Trans. Am. Geophys. Union, 66: 1067.

Tchalenko, J.S., 1970. Similarities between shear zones of different magnitudes. Geol. Soc. Am. Bull., 81: 1625–1640.